Large-scale structures forming in a cross flow: Particle Image Velocimetry conditional analysis

R. Camussi[+], A. Stella[*], G. Guj[+], T. A. Kowalewski[x]
[+]*Dipartimento di Ingegneria Meccanica e Industriale*
Universitá Roma Tre, Via della Vasca Navale 79, I-00146 Roma, Italy
[*]*Dipartimento di Ingegneria Meccanica e Aeronautica*
Universitá di Roma "La Sapienza", Via Eudossiana 18, I-00184 Roma, Italy
[x]*Polish Academy of Sciences, IPPT PAN, Swietokrzyska 21, PL-00049 Warszawa, Poland.*

Abstract.

A conditional Particle Image Velocimetry acquisition technique and averaging procedure are developed to study coherent structures formed by the interaction between a jet and a cross-stream. The experiment is conducted in a water tunnel, the water transversal jet is perturbed by a mechanical device. Measurements are performed at Reynolds number 100 and cross-flow velocity ratio ranging from 2.0 to 4.5. Sequences of images are acquired synchronously to the perturbation so that a statistical process may be applied to obtain average velocity and vorticity in a selected cross-section of the flow. The averaged fields and the instantaneous images together with flow visualizations by Laser Induced Fluorescence (LIF) technique are used to interpret behaviour of the large-scale vortices generated in the cross-flow experiment.

Key words: Particle Image Velocimetry, cross flow, coherent flow structures

1. Introduction

The study of jets exhausting in a cross-flow is an important issue for many physical problems and applications in engineering and environmental aspects such as flow control problems, thermal fatigue in pipeline junctions, mixing phenomena in the advection or dispersion of polluting fluids or fuel injection in an air cross-stream in non-premixed flame combustion. In all these cases, large-scale structures forming in the flow field have a strong effect on the overall behaviour determining the amount of mixing and relaxation time of the process. The importance of the subject has stimulated several studies in air and water facilities (see e.g. [8] for an exhaustive review of previous analyses). In the case of water experiments, most of the studies have been conducted by flow visualizations which, even if often of fundamental importance for preliminary understanding of the physical behaviours, lead to qualitative results. On the other hand, image processing techniques can deliver quantitative information about the investigated flow. The Particle Image Velocimetry (PIV) method offers one such possibility. The technique is based on the idea of taking couples of images separated by a known time delay Δt of a flow seeded with particles and illuminated by a laser light sheet. By a cross-correlation of

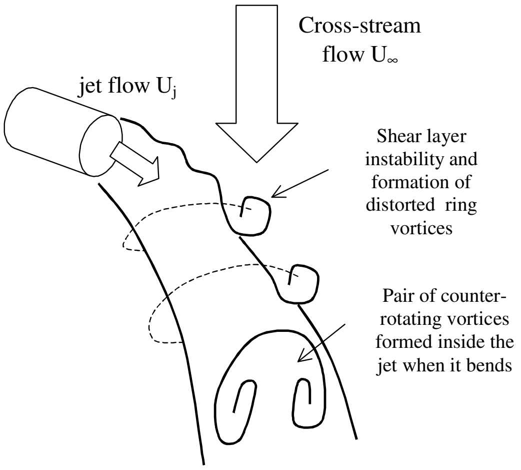

Fig. 1. A very simplified scheme of the main vortical structures forming as an effect of the interaction between the jet flow and the cross-stream

small sections of two images it is possible to compute the mean displacement of tracer particles. By moving the interrogation section step by step, the velocity vector field within the illuminated plane is obtained. As pointed out in [4], the PIV technique provides a good connection between the clear features observed by visualizations, and the need for a quantification of the velocity or vorticity magnitudes.

In the typical configuration, a jet issues from a circular orifice into a channel perpendicular to its main axis. The fluid flowing in the channel interacts with the jet bending it, and a number of characteristic fluid structures are formed. The problem is defined by the orifice diameter D_j, jet velocity U_j and unperturbed velocity of the channel flow U_∞. The two principal non-dimensional parameters which describe the problem are the jet to cross stream velocity ratio $R = U_j/U_\infty$ and the main stream Reynolds number $Re_j = U_\infty D_j/\nu$; ν is the kinematic viscosity of the fluid.

A simplified scheme of the typical fluid-dynamic structures is shown in Fig. 1. In particular we consider two basic flow structures. The first consists of the pair of counter rotating vortices and forms inside the jet flow, when it bends under the effect of the cross stream (see e.g. [2]). The second, a ring-like structure, forms at the upper shear layer of the jet as an effect of a destabilization mechanism of the Kelvin-Helmholtz type (see e.g. [1] and [3] for more details). In Figures 2 and 3, we give examples of planar flow visualizations of such structures. Specifically, in Fig. 2 the counter rotating vortices are visualized at several distances from the wall, whereas the shear layer oscillations are

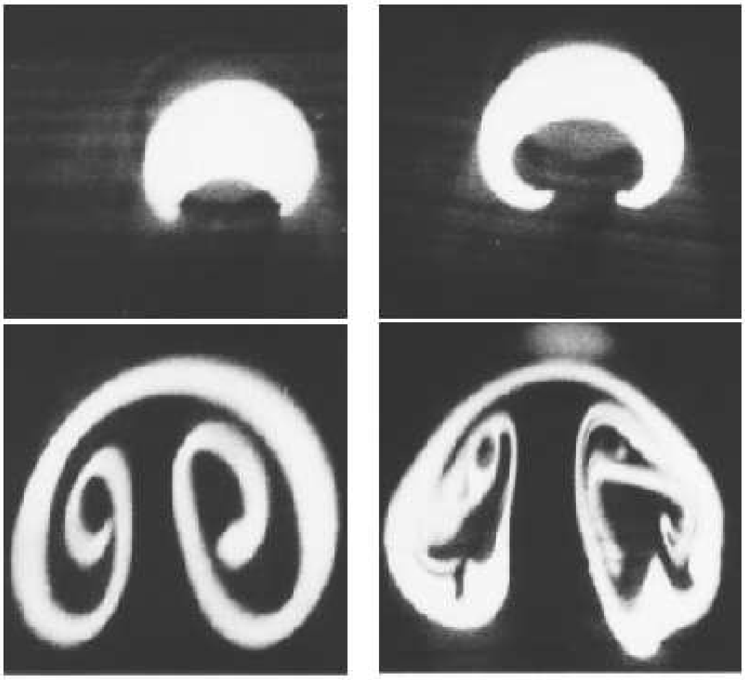

Fig. 2. Visualization of the counter rotating vortices forming within the jet flow observed at four different distances from the jet exit (increasing from left to right) . The plane of the photo is perpendicular to the jet axis; velocity ratio $R = 2$.

evidenced in Fig. 3.

From a physical viewpoint, one of the basic aspects of the problem needing clarification by more quantitative analyses, is the influence of both non-dimensional parameters, namely velocity ratio R and the Reynolds number, on the vorticity dynamics mechanisms and coherent structures evolution. In spite of extensive experimental efforts aimed at understanding these structures, the overall picture is still unclear. Indeed, previous quantitative analyses of such flow configuration were mainly based on hot wire anemometric measurements. However, these pointwise measurements do not give information on the general evolution of the fluid structures due to their local characteristics. Furthermore, they may be affected by significant errors, in particular in reverse flow conditions (see [4]). On the other hand, application of the PIV allows for full field velocity measurements and significantly increases the amount of data collected. Even if the applied PIV procedure only allows to measure the projection of the velocity field onto a plane,

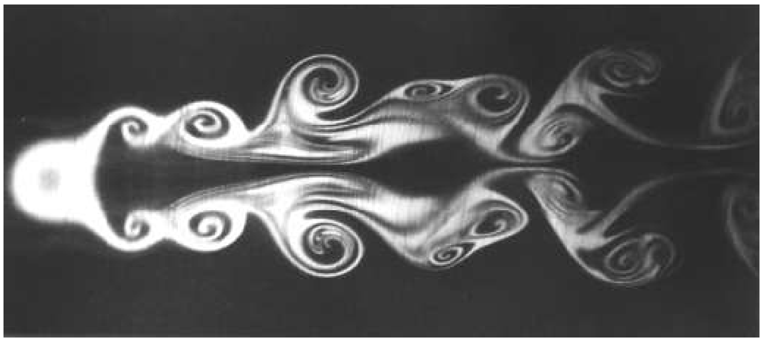

Fig. 3. Visualization of the vortices forming in the shear layer between the jet and the cross stream. The plane of the photo is parallel to the wall where the jet is flush mounted; velocity ratio $R = 2$.

i.e. two-dimensional fields, it appears as an optimal tool for analyzing the large scale structures forming in the cross flow at low Re_j.

In the present work, a new technique for phase averaging and conditional PIV acquisitions has been developed and applied to the cross-flow. The proposed technique is based on the idea that the mechanism of destabilization and formation of the coherent structures, which mostly influences the fluid dynamics, may be induced by a mechanical perturbation of the issuing jet. As will be described later in more detail, the external perturbation is synchronized with the PIV acquisitions. This allows us for an analysis of the mean fields by ensemble averages. In particular, the conditional technique permits to enhance the coherent structures and to analyse their characteristics and spatial evolution for different velocity ratios R.

We wish to emphasise that the low Re_j achieved in the present work has never been analysed before, even though such data appear to be crucial for comparisons with numerical simulations. Furthermore, the forcing-conditional methodology, as proposed in the present paper, has never before been applied to a cross-flow configuration.

The present paper is organized as follows: in Sec. 2 the experimental facility is described as well as the procedures adopted for the PIV acquisitions without jet perturbations. The conditional averaging technique adopted when the perturbation is active is described in Sec.3. Results and discussions are presented in Sec. 4 and the final remarks and conclusions are summarized in Sec. 5.

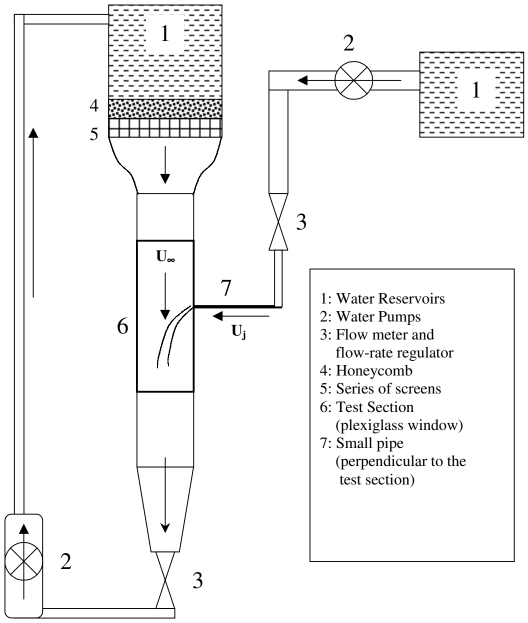

Fig. 4. Sketch of the experimental apparatus

2. Experimental facility and PIV system

2.1. Experimental facility

Experiments were carried out in a vertical water channel available at the Aerodynamics Laboratory of the Department of Mechanics and Aeronautics, of the University "La Sapienza" of Rome. The channel has a converging nozzle with a contraction ratio of 10. The test chamber of $0.5m$ in length has a square section of $0.1 \times 0.1m^2$. The mean velocities of the free stream and of the jet flow were evaluated from the flow rate measured by a flow meter. A water jet issues from a circular orifice $5mm$ in diameter located at one side of the test chamber. For PIV measurements, both the jet and the free stream fluid temperatures were monitored in order to control the buoyancy effects. A sketch of the experimental apparatus is shown in Fig. 4.

Preliminary measurements of the flow quality (turbulence level, flow uniformity, free stream velocity stability etc.) were conducted by Laser Doppler Anemometry. The free stream velocity was fixed at $0.02m/s$ in all tests, and the corresponding value of Re_j was 100. The velocity ratio R, which is the only dimensionless parameter that was varied,

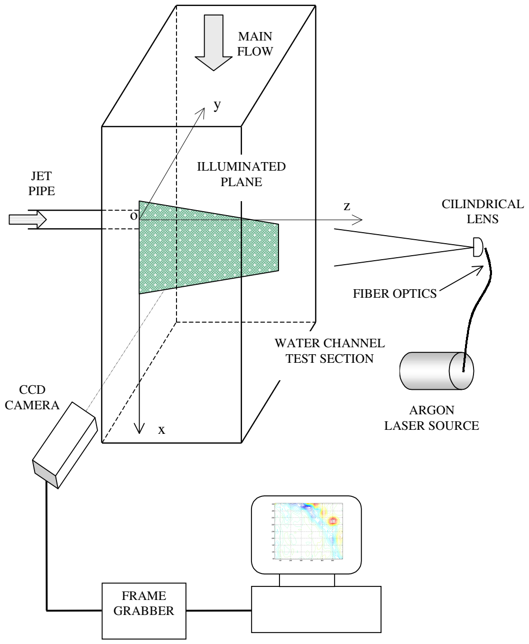

Fig. 5. A scheme of the PIV set up

ranged from 2 up to 4.5.

2.2. PIV system

A schematic representation of the PIV system is shown in Fig. 5. A $1mm$ thick light sheet was obtained by expanding a beam from a 2 Watt, continuous, Argon laser ($\lambda = 513\mu m$) through a cylindrical lens. The illuminating plane was placed in several positions within the test section. More specifically, the *longitudinal* velocity field was obtained by placing the light sheet on the jet symmetry plane perpendicular to the wall, and the *transverse* velocity field was obtained by placing the light sheet perpendicular to the jet axis. In the latter case, measurements were taken at three different axial distances from the jet issue ($x/D = 1.6$ for $R = 2$, $x/D = 3.6$ for $R = 3$ and $R = 4$ and $x/D = 5.6$ for $R = 3$ and $R = 4$).

Image acquisitions were achieved by a digital monochrome camera (SONY XC-77RR-CE CCD), with optical sensitive picture elements (pixels) arranged in a frame of 756 horizontal lines and 581 vertical columns. The size of a pixel is 11 x 11 μm. The camera operates in the interlaced frame integration mode, which gives the highest spatial resolution. The frame is divided into two fields, one containing the odd numbered lines and one the even ones. The electronic shutter of the camera was used. The exposure time of a single field was selected as a compromise, short enough to reduce particle blurring but long enough to collect a sufficient amount of scattered light. Hence, the shutter time was varied depending on the relative velocity R, and fixed at 15 ms for $R = 2$, $12ms$ for $R = 3$ and $9ms$ for $R = 4$ and 4.5. The images were acquired on-line by the 8-bit A/D converter of a VFG-100 image processing board. For the purposes of conditional PIV acquisition sequences of 4 images, 768 x 512 pixels, were periodically acquired at selected time intervals into the frame buffer and stored on a computer hard disk.

The mean diameter d of lycopodium particles added as tracers both to the jet and the cross stream was 30 μm. Their density ρ_p is only 31% of that of water. We assume that particles dispersed in the flow follow the flow streamlines. Hence, it was necessary to ensure that the particle velocity lag remained small compared to the main flow velocity. The terminal velocity of a particle due to gravity is given by:

$$V_g = g(\rho_p - \rho_f)d^2/18\mu \tag{1}$$

where ρ_f and μ are the density and viscosity of water, and g the gravity acceleration. For a lycopodium particle in water we obtain $V_g = 0.34mm/s$. The relaxation time of a lycopodium particle in water, defined as:

$$\tau = \rho_p d^2/18\mu \tag{2}$$

is equal to $1.5 \times 10^{-5} sec$. These values are satisfactory in terms of our experimental accuracy since V_g is about 1.5% of the mean stream velocity and τ corresponds to a cut-off frequency of 6.7 KHz, well above the frequency characteristic for the structure interaction.

According to the classical digital PIV approach ([5],[10]), the velocity is measured by applying a cross-correlation technique between pairs of successive images separated by a known time delay Δt. Small sections of both images, called *Interrogation Windows* (IW), are cross-correlated and the average spatial displacement of the particles is evaluated. The mean displacement is provided by the position of the cross-correlation peak and the velocity in the IW is finally obtained by dividing the displacement by the time interval Δt. The relative amplitude of the cross-correlation peaks with respect to the noise level is an indication of the measurement quality and is used as a criterion for the velocity vectors validation procedure. In the implemented PIV technique (proposed in [6]), pairs of images to be correlated are obtained using a single CCD video frame and extracting both fields corresponding to odd and even video lines. Hence, a minimum time delay between images was $\Delta t = 20ms$. This time interval can be increased by considering pairs of fields extracted from different frames of a sequence. Interrogation windows of 48 x 24 pixels, 50 % overlapped, were used to evaluate particle displacement. The matrix of the in-plane velocity vectors, whose point of application is the center of an IW, is composed of 31 rows in the horizontal direction and 21 columns in the vertical one. The scale factor is 1:0.098 for the longitudinal velocity fields and 1:0.107 for the transverse ones, i.e. 1 mm

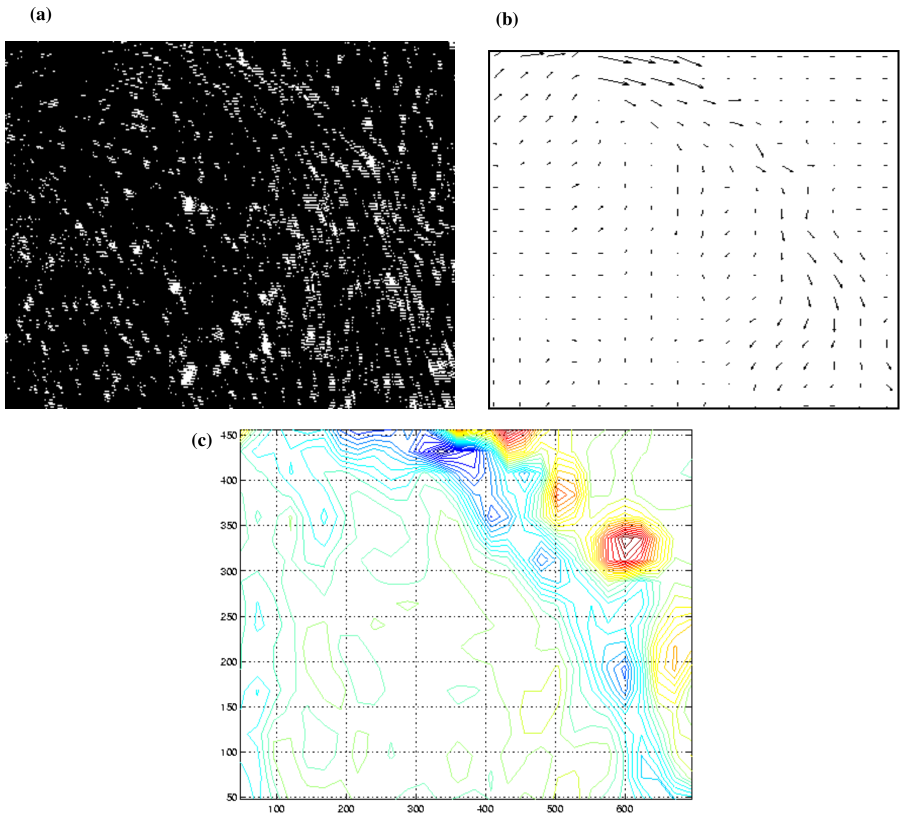

Fig. 6. An example of the post-processing procedure adopted to obtain an instantaneous vorticity contour from a PIV image acquired at $R = 3$. (a): raw image acquired from the CCD camera; (b): velocity vector field obtained from the cross-correlation procedure; (c): vorticity contour calculated from (b). Red colour indicates positive (counter-clockwise) vorticity, whereas blue colour indicates negative vorticity.

in physical space corresponds respectively to 0.098 mm and 0.107 mm on the sensor of the CCD camera. The spatial resolution in physical space is 2.4 mm for the longitudinal fields and almost 2.6 mm for the transverse ones. A two-dimensional discrete Fourier transform is applied to evaluate the cross-correlation function in the IW. The particle displacement is determined with a resolution of up to 1/2 pixel through interpolation, corresponding to about 0.05 mm. In order to improve the accuracy of this calculation, images are pre-processed to enhance the signal to noise ratio. The image enhancement produces a quasi binary image by equalising the variation of the particle intensity. This is so called local image binarization [6]. Hence, the final image contains uniformly bright particles on a black background. The minimum velocity V_{min} the system is able to resolve is given by the ratio between the minimum detectable displacement of particles and time interval Δt. For the present measurements we may assume $V_{min} = 2.5mm/s$. The maximum reliable displacement detectable by FFT based PIV evaluation is limited by the dimension of the interrogation window IW (see [7],[10]). In practice it does not exceed 1/2 of the IW size. In our case it corresponds to a maximum resolvable velocity V_{max} of about $114mm/s$ for the horizontal component and $57mm/s$ for the vertical one. The estimated dynamic range V_{max}/V_{min} of the available PIV system in the adopted experimental conditions is thus 22.5:1 for the horizontal velocity and 11.25:1 for the vertical one.

In addition, the accuracy of PIV is reduced by out of plane flow, which conveys particles across the light sheet. This causes a broadening of the cross-correlation peak, which diminishes the overall evaluation accuracy. In our experiments the third velocity component was estimated using measurements of the transversal field in the regions crossed by the jet flow. A reference normal velocity equal to 1/2 of that of the jet in the case $R = 4$ ($U_j \simeq 75\ mm/s$) was taken as the worst situation. The corresponding particle displacement perpendicular to the light sheet during Δt is about $0.5mm$, that is about 50% of the transversal dimension of the sheet. This condition exceeds the 1/4 criterion proposed in [7] and [10]. Previous tests [11], conducted using synthetic images representative of the random particle texture, indicated a relatively small influence of the optical noise caused by particle appearance and disappearance on the accuracy of PIV evaluation. In fact, a removal of up to 20-30% of the particles causes a decrease in accuracy below 3% for the displacement angle and 2.5% for the absolute displacement. As a matter of fact, the quality of the resulting longitudinal and transverse velocity fields appears to be generally high, since the number of non-physical vectors it was necessary to substitute by averages among the surrounding ones, was below 5%. It means that application of data validation procedures, such as using quality of the cross-correlation to filter the velocity field, was not crucial for content of the collected information.

An example of the post-processing procedure performed for the standard PIV analysis, is shown in Fig. 6: where (a) is the particle image, (b) is its corresponding velocity vectors field, and (c) shows the contour plot of the longitudinal vorticity amplitude.

2.3. Flow visualization

Flow visualization experiments were performed by the Laser Induced Fluorescence (LIF) method. The technique is based on the laser induced fluorescence of a colorant (fluorescein) which is mixed with the flow exhausting from the jet. The flow structures are observed within the laser light sheet illuminating selected cross-sections of the flow. This technique was very useful for qualitative flow analysis of our preliminary studies. In the present case, the laser sheet is obtained in the same manner as for the PIV analysis and also the plane positions adopted are the same as for the PIV measurements (planes perpendicular to the wall for the *longitudinal* cuts and perpendicular to the jet flow axis for the *transverse* ones). The image analysis is performed by standard video tape recording, using the CCD camera adopted for the PIV acquisitions. Examples of the results obtained by the LIF technique are presented in Figs. 2 and 3, where the white regions represent fluid coming from the jet (mixed with fluorescein), and the darker ones represent the external fluid.

3. Conditional acquisition and post-processing

A conditional acquisition procedure was implemented in order to collect a series of images taken phase-locked to coherent structures position. To synchronise the acquisition time with the structure appearance, the jet velocity was mechanically perturbed. The controlled jet flow perturbations are obtained by squeezing the flexible supply pipe. The perturbation frequency used, f_D, is that of the preferred destabilization mode of

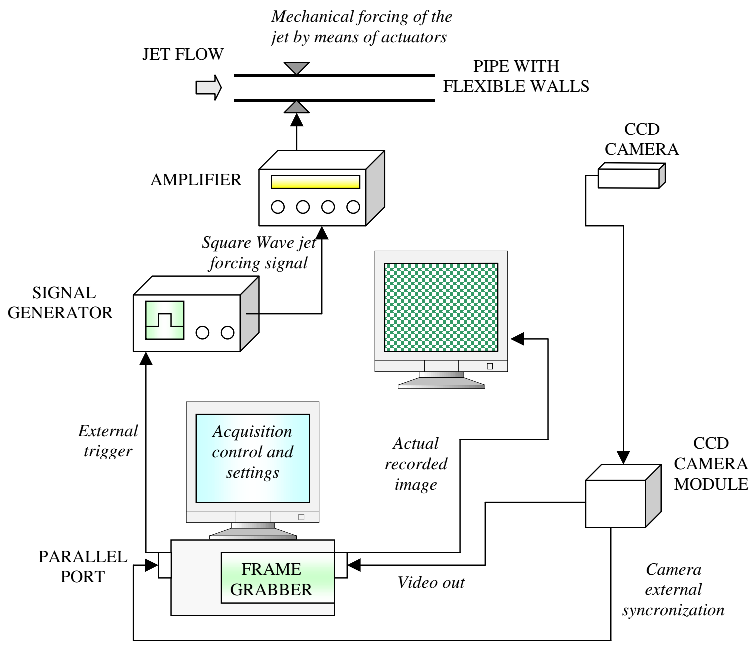

Fig. 7. Setup adopted for the conditional acquisitions

Case	f_D (Hz)	St
$R = 2$	10	0.63
$R = 3$	3.9	0.32
$R = 4$	5	0.63

Tab. 1. Frequency adopted for the mechanical forcing (f_D). The corresponding non-dimensional Strouhal numbers (St) are also reported.

the investigated cross-flow configuration. This frequency was determined in separate experiments with an unperturbed jet. Selected values of f_D are listed in Tab. 1 along with the resulting non-dimensional parameter, the Strouhal number, defined as $St = f_D D_j / U_j$.

The sketch of the experimental set-up for the PIV conditional acquisition is shown in Fig. 7. The synchronization between jet external forcing and image capturing is controlled by a computer. The external synchronization signal provided by the CCD video camera module is used as a time base to conditionally trigger a signal generator. The trigger signal generates a square wave train (50% duty cycle) with the appropriate frequency f_D ensuring phase-locking with image acquisition timing.

The timing chart of jet forcing and images acquisition is shown in Fig. 8. The time interval Δt_{PT} between the beginning of jet excitation signal and the first image acquisition (pre-trigger time), as well as the delay Δt_{IMG} between the four images of a sequence, determine the phase-delay between the acquired images and the position of the coherent structures. The first parameter was not changed during the present campaign of measurements and set at $10s$. The time shift Δt_{IMG} was maintained at $200ms$ in all the tested cross-flow conditions, with the exception of the case $R = 3$ for which further acquisitions with $\Delta t_{IMG} = 100ms$ and $\Delta t_{IMG} = 300ms$ were carried out to assess the related phase variation.

Due to the external perturbations, quasi-periodic fluid structures tend to appear (see the sketch in Fig. 1 and the visualization in Fig. 3) and a large number of images have to be collected and averaged to perform a reliable statistical analysis. Our conditional statistic is based on about 50 realizations per image (for each flow condition 200 images were acquired). In Tab. 2, a summary of the analysed flow conditions is reported. Each image has been processed to achieve the instantaneous velocity and vorticity field and, for each flow condition, the ensemble averages were performed over the fields corresponding to the same phase delay.

R	δt (sec)	LS
2	200	Long. and Transv.
3	100, 200, 300	Long. and Transv.
4	200	Long. and Transv.
4.5	200	Longitudinal

Tab. 2. Flow conditions examined with the external forcing: δt denotes the time between conditioned images, and LS the light sheet position

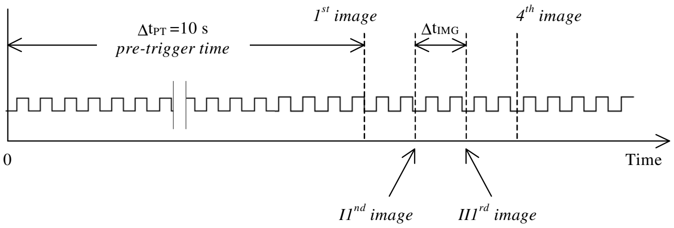

Fig. 8. Time chart of jet forcing and image acquisition

4. Results and discussion

As pointed out by Kelso et al. [8], the ensemble average makes it possible to eliminate random fluctuations, thus facilitating the study of the coherent structures. The average vorticity fields allow us to analyse the structures which are directly correlated to the excitation mechanism of the shear layer.

In Figure 9, an example of the ensemble average obtained by applying the external jet excitation is shown. The figure is obtained for a velocity ratio $R = 3$ and a time delay between images of $300ms$. It is evident that the vorticity contours at a known phase delay allows for the analysis of the evolution of the coherent structures. More specifically, since the images are obtained with the light sheet positioned perpendicular to the wall, the presence and evolution of the ring-like structures forming in the shear layer can be observed. The difference between the vorticity contour at different time delays is an evidence of the unsteadiness of the phenomenon, especially at relatively large distances from the jet exhaust. Indeed, one can clearly observe the formation of a strong ring vortex at the exit of the jet. At the upper side it has the same vorticity as the wall boundary layer and on the lower side its vorticity has an opposite sign. This appears as a steady structure which is always observed in any flow condition.

At a distance of few diameters from the jet, the destabilization of the upper shear layer is clearly observed with the formation of annular structures. Their *signature* is evidenced

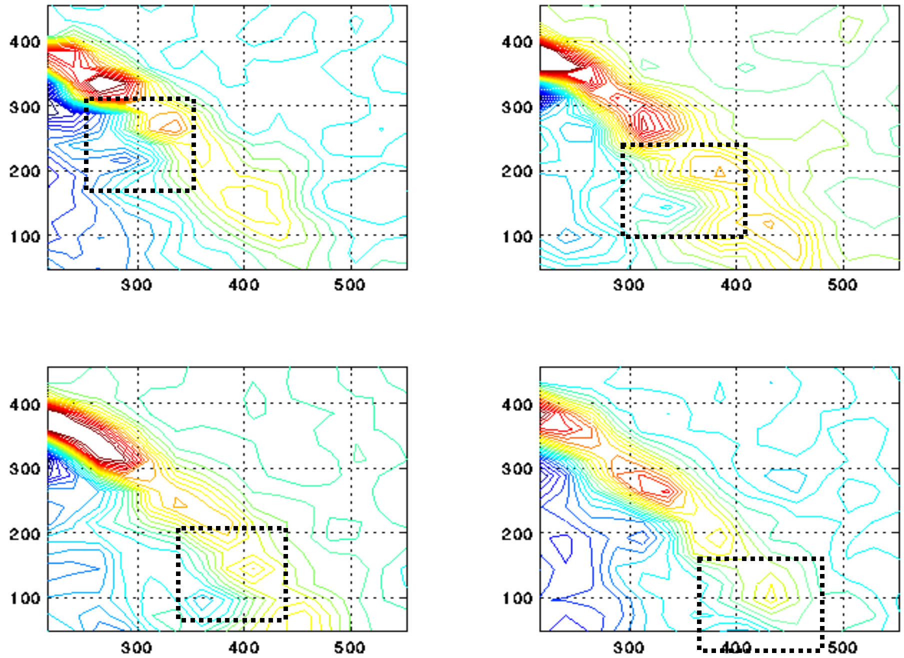

Fig. 9. Vorticity contour plots illustrating evolution of a ring vortex observed at time interval of $300ms$. The contour plots of mean longitudinal vorticity are obtained by the conditional average of 50 images. The light sheet is perpendicular to the wall; velocity ratio $R = 3$.

by couples of positive or jet-like (counter-clockwise on the upper side) and negative or wake-like (clockwise on the lower side) vorticity. Taking into account that the positive and negative values of the vorticity amplitude are reported with the same resolution, it seems evident that the vorticity of the upper shear layer is stronger (for $R = 3$) than that observed in the lower one. This is a typical behaviour observed for $R > 2$ and further discussions will be given later. Nevertheless, even with different magnitudes, it seems that there is always a coupling between upper (with positive vorticity) and lower (with negative vorticity) structures. This is an indication of the formation of small ring vortices with a weaker vorticity on their lower side (note that this aspect is very difficult to observe in flow visualizations). Therefore, the shear layer instability on the upper side, leads to the formation of a strong vortex with positive vorticity which detaches from the steady structures at the jet exit. As soon as it is formed, a secondary vortex with weaker vorticity of opposite sign is also formed and it moves coupled to the first one. This appears to be the *signature* of a ring vortex. Taking into account the magnitude of

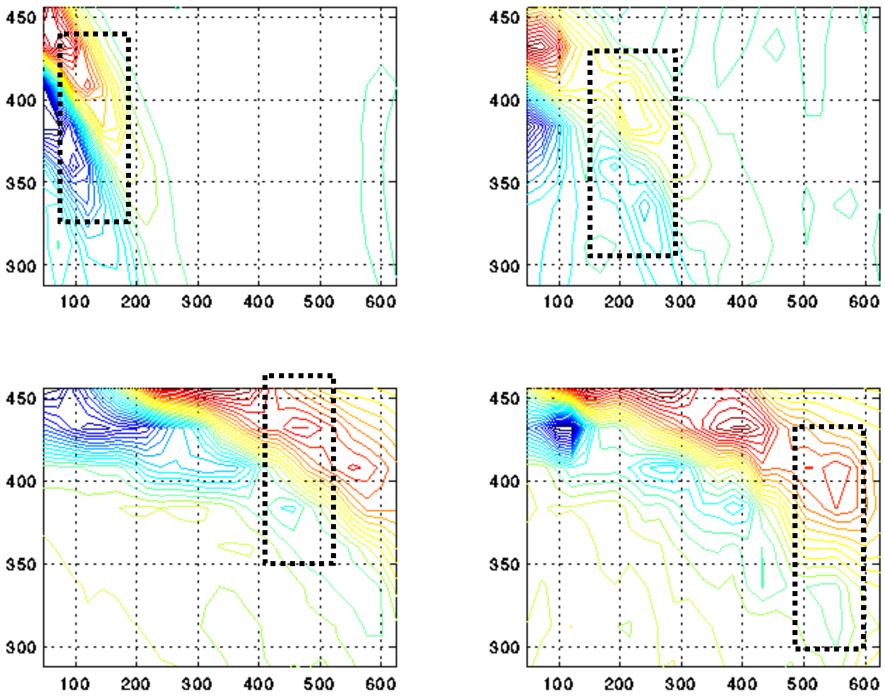

Fig. 10. Vorticity contours at a time phase of $1200ms$ from the start of the perturbation (see Fig. 5). The contour plots of mean longitudinal vorticity are obtained by the conditional average of about 50 images. The four plots correspond to $R = 2$, $R = 3$, $R = 4$ and $R = 4.5$ (from left to right). The light sheet is perpendicular to the wall. The rectangular window highlights the presence of a couple of vortices with positive and negative vorticity (signature of ring-like structures).

the mean velocity of the cross stream and the time delay between the images, the use of the conditional averages allows us to follow the evolution of a ring during a total time interval of $900ms$. This is shown by the highlighted regions in the figures.

It is also observed that when the vortex is sufficiently far from the jet, the positive vorticity of the upper side decreases faster than the negative one on the lower side. As suggested by Andreopulos [3], it is expected that very far from the jet, the negative vorticity prevails. This phenomenon can not be observed here due to the transition to turbulence and the effect of viscous diffusion.

Analogous observations were done for the other cases at $R > 3$ (not reported here for brevity). However, several significant differences are found with respect to the observations at $R = 2$. In particular the main transitional behaviour seems to be the passage from a steady to an unsteady state of the ring-like structures of the shear layer. The effect of the velocity ratio R, may be better understood by the analysis in Fig. 10. Here, a sequence of four images corresponding to the same phase delay but at four different values of R are reported (from $R = 2$ up to $R = 4.5$). As pointed out above, the formation of a strong ring vortex at the exit of the jet is confirmed for each R, thus supporting the idea that this is the only vortical structure which conserves a steady state independently of the velocity ratios. Also, the formation of jet-like structures (of counter-clockwise vorticity) on the upper side of the jet is always observed independently of R. This is an important point since it seems in partial contrast with results of flow visualizations performed on the same flow configuration and experimental apparatus (see [9] for details). Indeed, as shown in Fig. 3, at $R = 2$ the vorticity seems to be entirely counter-clockwise directed (wake-like), whereas the PIV results show that jet-like vorticity is present even for very low R. Indeed, it is expected that when a scalar (e.g. coloured dye) is used for the flow visualization it may be completely entrained within the vortices of the largest vorticity magnitude. For the case $R = 2$, the largest vorticity is the negative one, whereas for larger R the jet-like vorticity prevails. It was shown in the previous figure and as it is enhanced in Fig. 10. In addition to the ring formed at the jet exhaust, far from the wall ring vortices are formed with *signature* given by the couple of positive and negative vorticies. It is confirmed for investigated range of the velocity ratio R.

Nevertheless, the increase in R leads to an increase in the positive vorticity on the upper side of the shear layer, which prevails on the negative vorticity of the lower side. Comparing the results presented here with additional analysis by flow visualization, it appears that a transitional behaviour occurs at $R = 3$. In fact, for this velocity ratio, the positive and negative vorticity amplitudes are of comparable magnitude. Furthermore, as already pointed out, the value $R = 3$ seems also to be the transitional threshold between steady and unsteady formation of rings.

The analysis of the averaged vorticity contour corresponding to the transverse light sheet substantially indicates the steady nature of the counter rotating vortices. As an example, in Fig. 11 we report the averaged vorticity for a fixed position and time delay, changing the velocity ratio R. It is shown that an increase in the velocity ratio leads to a faster formation of the vortex pair which, in any case, are formed even for lower R. The conditional analysis in this case is less effective then for the longitudinal cases, nevertheless confirms previous results obtained by flow visualization (comp. [8] and [9], and see Fig. 2).

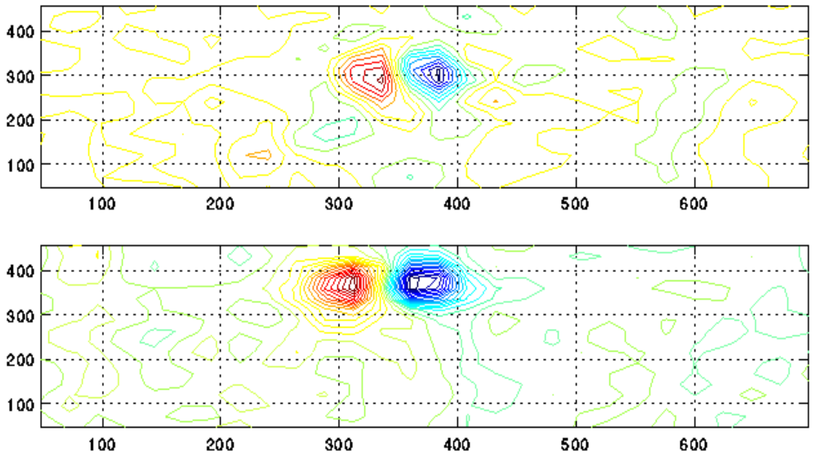

Fig. 11. Vorticity countours at a time phase of $1200ms$ from the start of the perturbation. The position of the light sheet parallel to the wall, close to the jet exit. The contour plots of mean vorticity are obtained by the conditional average of about 50 images. The two plots correspond to velocity ratios $R = 3$ and $R = 4$ (upper and bottom subfigure, respectively).

5. Conclusions and final remarks

A conditional Particle Image Velocimetry acquisition technique was developed and applied to study large scale structures forming by the external destabilization of a jet issuing into a cross flow. The experimental analysis was carried out in a water tunnel at very low Reynolds number ($Re_j = 100$) and at various jet-to-cross stream velocity ratios (R from 2 up to 4.5). The acquisition conditioning has been performed by mechanical excitation of the jet with a frequency equal or multiple of the typical one for the shear layer instability. The forcing allowed for synchronized acquisition of images at a given phase. The main results achieved may be summarized as follows:

- The jet forcing leads to the enhancement of the coherent structures, especially for vortical structures generated in the shear layer of the jet.
- The conditional acquisition technique enabled ensemble averages of the velocity and vorticity fields to be performed, leading to averaged 2D fields which allows for the analysis of the transitional mechanisms in the shear layer by increasing R.
- The case $R = 3$ seems to be a transitional condition between a steady state ($R = 2$) and unsteady conditions. At any rate, the formation of a steady ring vortex at the jet exit is always observed.
- At any flow condition, ring vortices also form far from the jet exit. It is observed

that the flow condition corresponding to about $R = 3$ is a limit which separates two regimes: for $R < 3$ most of the vortical ring like structures are characterized by prevailing wake-like vorticity whereas for $R > 3$ the jet-like vorticity is dominant. However, in partial contrast with flow visualization results, the jet-like vorticity structures are always observed, independently of the R magnitude.

- The pair of counter rotating vortices is always seen to form as soon as the jet flow starts to bend under the effect of the cross stream. These appear as steady structures whose vorticity, for fixed distances from the jet, increases for increasing R.

References

1978

[1] Yule A.J.: Large-scale structure in the mixing layer of a round jet, J. Fluid Mech., 89, 413-432.

1984

[2] Broadwell J.E. and Breidenthal R.E.: Structure and mixing of a transverse jet in incompressible flow, J. Fluid Mech., 148, 405-412.

1985

[3] Andreopulos J.: On the structures of jets in cross-flows. J. Fluid Mech., 157, 163-197.

1991

[4] Adrian R.J.: Particle imaging techniques for experimental fluid mechanics, Ann. Rev. Fluid Mech., 23, 261-304.

[5] Willert, CE.: Gharib M Digital particle image velocimetry. Exp. in Fluids, 10, 181-193.

1993

[6] Hiller W., Koch S., Kowalewski T.A., Stella F, Onset of natural convection in a cube, J. Heat and mass transfer, 16(13), pp.3251-3263.

[7] Keane R.D., Adrian R.J.: Theory of cross-correlation analysis of PIV images. Applied Scientific Research, 49, 191-215.

1996

[8] Kelso, R.M., Lim, T.T. and Perry, A.E.: An experimental study of round jets in cross flows. J. Fluid Mech., 306, 111-144.

1998

[9] Camussi R. , Guj G., Leone A.: Experimental analysis of jets in cross-flow at low and moderate Reynolds number. in 8th International Symposium on Flow Visualization, Sorrento (Italy), edts. G.M. Carlomagno and I. Grant, CD ROM Proceedings ISBN 0953399109, Edinburgh, ODE, pp. 066.1-10.

[10] Raffel M., Willert C., Kompenhans J.: Particle image velocimetry. Berlin, Springer.

[11] Quenot G.M., Pakleza J., Kowalewski T.A. Particle image velocimetry with optical flow, Exp. in Fluids, Vol. 25, pp. 177-189.